SCIENCE CHINA Materials ARTICLES

mater.scichina.com link.springer.com

Published online 30 September 2020 | https://doi.org/10.1007/s40843-020-1475-2
Sci China Mater 2021, 64(4): 861–869

Hollow cobalt-nickel phosphide nanocages for efficient electrochemical overall water splitting

Zhiyuan Wang[1,2], Jia Yang[2], Wenyu Wang[2], Fangyao Zhou[2], Huang Zhou[2], Zhenggang Xue[2], Can Xiong[2], Zhen-Qiang Yu[1*] and Yuen Wu[2*]

ABSTRACT **A low-cost, highly efficient and strong durable bifunctional electrocatalyst is crucial for electrochemical overall water splitting. In this paper, a self-templated strategy combined with *in-situ* phosphorization is applied to construct hollow structured bimetallic cobalt-nickel phosphide ($CoNiP_x$) nanocages. Owing to their unique hollow structure and bimetallic synergistic effects, the as-synthesized $CoNiP_x$ hollow nanocages exhibit a high electrocatalytic activity and stability towards hydrogen evolution reaction in all-pH electrolyte and a remarkable electrochemical performance for oxygen evolution reaction in 1.0 mol L^{-1} KOH. Meanwhile, with the bifunctional electrocatalyst in both anode and cathode for overall water splitting, a low voltage of 1.61 V and superior stability are achieved at a current density of 20 mA cm^{-2}.**

Keywords: bimetallic cobalt-nickel phosphide, hollow nanocage, electrochemical water splitting, all-pH electrolyte

INTRODUCTION

The increasing energy consumption and serious environmental problems have forced us to develop sustainable and environment-friendly energy systems [1,2]. Among numerous renewable energies, hydrogen (H_2) is regarded as one of the promising energy carriers to replace fossil fuels, owing to the high energy efficiency and non-polluting product [3,4]. In recent decades, the fast development and wide application of H_2 fuel cells have led to a huge demand for H_2 preparation. Electrochemical water splitting, a clean and efficient technology, is considered as one of the most promising approaches to obtain H_2 with high purity. However, because of the sluggish reaction kinetics and non-negligible overpotential (η) for both hydrogen evolution reaction (HER) and oxygen evolution reaction (OER) during water electrolysis [5–8], the large-scale H_2 preparation is seriously restricted, which has driven the exploration of high-efficiency electrocatalysts. Nowdays, the most widely used electrocatalysts for HER and OER are noble metals and their oxides, such as platium (Pt) [9,10], iridium (Ir) [11,12], iridium dioxide (IrO_2) [13,14] and ruthenium (Ru) [15–17]. Unfortunately, the scarcity and high-costs hinder their industrial applications. Therefore, to develop bifunctional electrocatalysts with low-cost but high activity and stability towards both OER and HER is extremely urgent [18–20].

In recent years, transition-metal oxides and corresponding transition metal phosphides [21–24], sulfides [25,26], nitrides [27,28], and selenides [29–31] have been extensively studied as non-precious bi-functional electrocatalysts for overall water-splitting. In particular, transition metal phosphides, especially bimetallic transition metal phosphides have attracted significant attentions as bi-functional electrocatalysts for water-splitting owing to their remarkably enhanced catalytic activities [32,33]. To maximize the electrochemical performance of the catalysts, endowing the electrocatalysts with hollow nanostructures is regarded as an effective approach, which can significantly increase their specific surface areas and expose more reactive sites [34–37]. Moreover, the ion diffusion length and transport resistance for water splitting can be effectively reduced by their large void spaces, which has been fully demonstrated by previous studies [38–40]. Therefore, the rational design of bimetallic transition-metal phosphides with hollow nanostructures is of great significance for improving their electrocatalyitc activities towards both HER and OER.

Encouraged by the above analysis, a hollow structured

[1] School of Chemistry and Environmental Engineering, Shenzhen University, Shenzhen 518060, China
[2] School of Chemistry and Materials Science, Hefei National Laboratory for Physical Sciences at the Microscale, University of Science and Technology of China, Hefei 230026, China
* Corresponding authors (emails: zqyu@szu.edu.cn (Yu ZQ); yuenwu@ustc.edu.cn (Wu Y))

bimetallic cobalt-nickel phosphide ($CoNiP_x$) was constructed *via* a self-templated strategy combined with the subsequent *in-situ* phosphorization. The as-synthesized $CoNiP_x$ hollow nanocages exhibited an excellent pH-universal electrocatalytic activity towards HER in all of the basic, neutral and acidic electrolytes, which is comparable to the commercial 20% Pt/C. Moreover, a superior OER catalytic activity in basic electrolyte was obtained, when the current density was 50 mA cm^{-2}, and a low overpotential of 320 mV was achieved. Specifically, the as-synthesized $CoNiP_x$ was further used as the bifunctional electrocatalyst in both anode and cathode for electrochemical water-splitting. A high current density of 20 mA cm^{-2} was obtained when the cell voltage was as low as 1.61 V. After 12 h measurement, the slightly decreased current density indicated an excellent durability.

EXPERIMENTAL SECTION

Materials

Cobalt acetate tetrahydrate ($Co(OAc)_2{\cdot}4H_2O$, 99.5%), nickel nitrate hexahydrate ($Ni(NO_3)_2{\cdot}6H_2O$, 99%), polyvinylpyrrolidone (PVP, M_w = 40,000), sodium hypophosphite monohydrate ($NaH_2PO_2{\cdot}H_2O$, 99%), methanol, potassium hydroxide (KOH, ≥ 85.0%), sulfuric acid (H_2SO_4, ≥ 96.0%), instant premixed granules of phosphate buffered saline (PBS, pH 7.4) were purchased from Shanghai Chemical Reagents. All of the chemicals used in this experiment were analytical grade and used without further purification. Deionized (DI) water from a Milli-Q System (Millipore, Billerica, MA) was used in all experiments. Carbon paper (Toray, TGP-H-60) and graphite powder were purchased from Alfa Aesar.

Synthesis of cobalt acetate hydroxide nanoprisms

$Co(OAc)_2{\cdot}4H_2O$ (1.28 g) and 3.5 g of PVP were dissolved into 200 mL of ethanol with continuous stirring at room temperature to form a clear pink solution. Then the solution was transferred into a 500-mL round-bottom flask and heated to 85°C under refluxing conditions. After reacting for 24 h, the precipitate was collected by centrifugation at 9000 rpm, washed with ethanol several times and dried at 80°C under vacuum overnight.

Synthesis of Co-Ni LDH

The prepared cobalt acetate hydroxide nanoprism precursors were dispersed into 200 mL of ethanol in a 500-mL round-bottom flask under sonication. Then 0.55 g of $Ni(NO_3)_2{\cdot}6H_2O$ was added and stirred for 30 min. Then, the mixture was refluxed at 85°C for 6 h. After cooling to room temperature, the product (Co-Ni LDH) was collected by centrifugation at 9000 rpm, washed with ethanol several times and dried at 60°C under vacuum overnight.

Synthesis $CoNiP_x$ hollow nanocages

The prepared Co-Ni LDH and 1 g of $NaH_2PO_2{\cdot}H_2O$ were placed at two positions of the tube furnace in two porcelain boats and then heated at 300°C for 3 h in Ar atmosphere. After cooling down to room temperature, the $CoNiP_x$ hollow nanocages were obtained.

Characterization

Powder X-ray diffraction (XRD) patterns of the samples were recorded on a Rigaku Miniflex-600 operating at 40 kV voltage and 15 mA current with Cu Kα radiation (λ = 0.15406 nm). Transmission electron microscopy (TEM) images were recorded on a Hitachi-7700 working at 100 kV. The high-resolution TEM (HRTEM), high angle annular dark field-scanning transmission electron microscopy (HAADF-STEM) and energy dispersive X-ray spectroscopy (EDS) mapping were recorded by a Titan ETEM microscope (FEI) with a spherical aberration corrector working at 200 kV. The scanning electron microscopy (SEM) was performed on JSM-6700F. The inductively coupled plasma-optical emission spectroscopy (ICP-OES) was performed on Optima 7300 DV. X-ray photoelectron spectroscopy (XPS) was collected on a scanning X-ray microprobe (PHI 5000 Verasa, ULAC-PHI, Inc.) using Al Kα radiation with the C 1s peak at 284.8 eV as the internal standard.

Electrochemical measurements

All measurements were performed by a CHI 760E electrochemical workstation with a standard three-electrode system at room temperature, with the $NiCoP_x$ hollow nanocages coated on carbon paper, Pt mesh, and Ag/AgCl (saturated KCl) electrode as the working, counter, and reference electrodes, respectively. HER tests were carried out in 0.5 mol L^{-1} H_2SO_4 solution, 1.0 mol L^{-1} KOH solution and 1.0 mol L^{-1} PBS solution, respectively. The measured potentials were converted to reversible hydrogen electrode (RHE) using the following equation: $E(RHE) = E(Ag/AgCl) + 0.197\ V + 0.059pH$. The linear sweep voltammetry (LSV) curves were recorded at a scan rate of 5 mV s^{-1}. Electrochemical impedance spectroscopy (EIS) was performed from the frequency of 100 kHz to 0.1 Hz with a 10-mV alternating current voltage amplitude at different applied potentials. Before the electrochemical measurement of HER, the electrolytes

(0.5 mol L^{-1} H_2SO_4, 1.0 mol L^{-1} PBS and 1.0 mol L^{-1} KOH) were degassed by bubbling pure hydrogen for 30 min. OER tests were recorded in 1.0 mol L^{-1} KOH, and before OER, the KOH solution was degassed by bubbling pure Ar for 30 min.

RESULTS AND DISCUSSION

The preparation procedure is schematically illustrated in Fig. 1a. The cobalt acetate hydroxide nanoprism precursors were firstly synthesized by a surfactant-mediated method [41], which possessed an average size of 400 nm with a smooth surface (Figs S1, S2). Then the precursors reacted with nickel nitrate in ethanol under reflux, forming an ultrathin Co-Ni layered double hydroxide (LDH) on the surface. As the reaction continued, the inner precursors would be gradually dissolved and finally generate a hollow structured Co-Ni LDH (Fig. S3). Finally, the hollow structured Co-Ni LDH was chemically converted into Co-Ni bimetalic phosphides ($CoNiP_x$) by annealing with sodium dihydrogen hypophosphite (NaH_2PO_2) at 300°C under argon. The SEM images shown in Fig. 1b, c reveal that all the structures of $CoNiP_x$ are well maintained, and no obvious damage and collapse can be observed. All the $CoNiP_x$ exhibit a hierarchical structure with numerous curved nanosheets on the surface. As shown in Fig. 1d and Fig. S4, TEM images reveal a hollow structure of $CoNiP_x$ with ultrathin nanosheets assembling the shells, the thickness of the shell is about 15 nm. In particular, many homogeneous nanoparticles can be observed on the surface of the nanosheets (Fig. 1d, Figs S5, S6), which were proved to be $CoNiP_x$ nanocrystals with the assistance of HRTEM (Fig. S5). In the HRTEM image shown in Fig. 1e, three types lattice fringes with interplanar distances of 0.202 nm (Fig. 1f), 0.167 nm (Fig. 1g) and 0.249 nm (Fig. 1h) can be observed, which are in good agreement with the (201), (002), and (111) planes of $NiCoP_x$, respectively [42,43], confirming the successful synthesis of $NiCoP_x$. As exhibited in Fig. 1i and Fig. S6, the HAADF-STEM images further confirm the hollow feature, and the corresponding EDS mapping (Fig. 1j–m) demonstrates the uniformly distributed P, Co and Ni throughout the hollow nanocages.

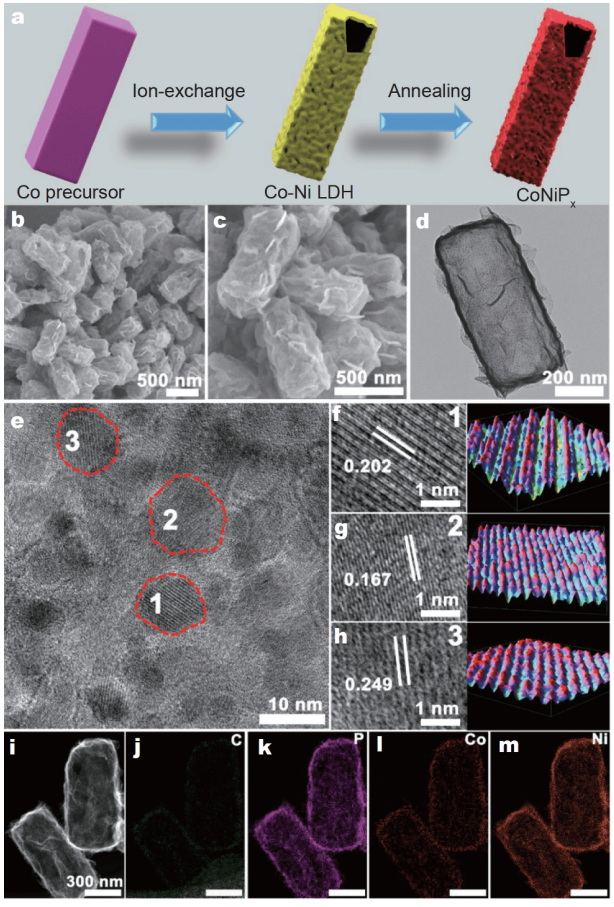

Figure 1 (a) Schematic illustration of the formation of the Co-Ni bimetalic phosphides. (b, c) SEM images of the synthesized $CoNiP_x$ hollow nanocages with different magnifications. (d) TEM and (e) HRTEM images of the synthesized $CoNiP_x$ hollow nanocage. (f–h) The magnified HRTEM images and the corresponding 3D overlapping Gaussian-function fitting maps. (i–m) HAADF-STEM image and the corresponding EDS elemental mapping images for the $CoNiP_x$ hollow nanocages.

The crystallinity of $CoNiP_x$ and control samples were studied by XRD, as exhibited in Fig. 2a. The peaks centered at 41.0°, 47.6°, and 54.7° are ascribed to the (111), (210), and (002) planes of $NiCoP_x$ (PDF: 01-071-2336) [42,44], and there are still some peaks corresponding to the impurity phases. The control samples of NiP_x and CoP_x were confirmed to be Ni_2P (PDF: 03-0953) and Co_2P (PDF: 54-0413). To confirm the molar ratio of the Co, Ni and P in $CoNiP_x$, ICP-OES was applied and the obtained molar ratio is 1:0.96:1.34, which is very close to the theoretical value of $CoNiP_x$. XPS was applied to investigate the surface chemical composition of $CoNiP_x$ and the oxidation states of the Co and Ni. The survey scan (Fig. S7a) of $CoNiP_x$ further confirms the presence of P, Co, Ni, O, and C in the product, which is in good agreement with the EDS mapping. Two obvious peaks at 781.3 and 797.7 eV in high-resolution Co 2p spectrum shown in Fig. 2b are assigned to the Co $2p_{3/2}$ and Co $2p_{1/2}$, and the peaks located at 785.7 and 803.6 eV are ascribed to the satellite peaks of Co $2p_{3/2}$ and Co $2p_{1/2}$, which are corresponding to the Co^{2+} and Co^{3+} species in $CoNiP_x$. In addition, the peak at 777.7 eV (Fig. 2b) is attributed to the

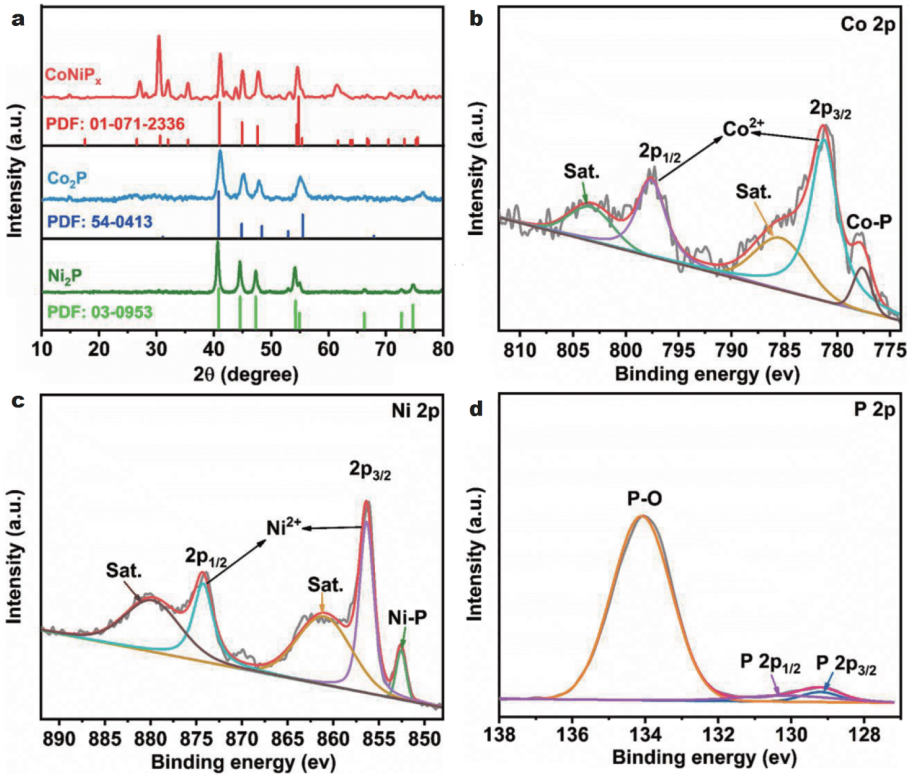

Figure 2 (a) XRD patterns of NiCoP$_x$, Co$_2$P and Ni$_2$P. High-resolution XPS spectra of the Co 2p (b), Ni 2p (c) and P 2p (d) for the CoNiP$_x$ hollow nanocages.

Co–P bond [22,43,45,46]. Similarly, in the high-resolution Ni 2p XPS spectrum (Fig. 2c), the obvious peak at 856.3 eV with a satellite peak at 861.2 eV is related to the spin-orbit splitting value of Ni 2p$_{3/2}$, and the peak at 874.3 eV with a satellite peak at 880.1 eV is attributed to the spin-orbit splitting value of Ni 2p$_{1/2}$, indicating the existence of Ni^{2+} and Ni^{3+} species. Moreover, the peak located at 852.6 eV in Fig. 2c indicates the formation of Ni–P bond [22,43,45,46]. Fig. 2d exhibits the XPS spectrum for P 2p, and the obvious peak at 134.1 eV is assigned to the surface P–O species because of the exposure to air. The other two peaks at 129.2 and 130.2 eV can be indexed to the P–Co and P–Ni species in CoNiP$_x$, which agree well with the 777.7 eV in Co 2p and 852.6 eV in Ni 2p, respectively [22,43,45,46]. The C 1s peaks at 288.6, 285.6 and 284.6 eV (Fig. S7a) are ascribed to O–C=O, C–O and C–C species, respectively [22]. Similarly, XPS spectra of the Co$_2$P and Ni$_2$P were also analyzed carefully in Figs S8, S9, which demonstrate the existence of Co, P and Ni, P in Co$_2$P and Ni$_2$P, respectively. The high resolution XPS spectra of Co$_2$P and Ni$_2$P both exhibit the same position peaks of Co 2p and Ni 2p in CoNiP$_x$, which indicates the Co species and Ni species in Co$_2$P and Ni$_2$P are same with those in CoNiP$_x$. In addition, the obvious peaks near 134 eV can also be found in high-resolution P 2p of Co$_2$P and Ni$_2$P, which are attributed to the P–O species. The other two peaks near 129 and 131 eV are ascribed to the Co–P and Ni–P species, respectively.

The electrochemical performance of the CoNiP$_x$ hollow nanocages towards HER was investigated *via* a standard three-electrode method in 1.0 mol L^{-1} KOH, 1.0 mol L^{-1} PBS, and 0.5 mol L^{-1} H_2SO_4, respectively. As a comparison, Co$_2$P, Ni$_2$P, and the commercial 20% Pt/C were used as the references. The LSV curves of the electrocatalysts shown in Fig. 3a were measured in 0.5 mol L^{-1} H_2SO_4 with a scan rate of 10 mV s^{-1}. As expected, the HER catalytic activity of the CoNiP$_x$ hollow nanocages is worse than commercial 20% Pt/C, but much better than that of the contrast Co$_2$P and Ni$_2$P. At a current density of 10 mA cm^{-2}, the overpotential of the CoNiP$_x$ hollow nanocage is 54 mV, and it is superior to 104 mV of Co$_2$P and 124 mV of Ni$_2$P. The corresponding Tafel slope of the CoNiP$_x$ hollow nanocages in Fig. 3b is 51 mV dec^{-1}, also smaller than those of Co$_2$P (62 mV dec^{-1}) and Ni$_2$P

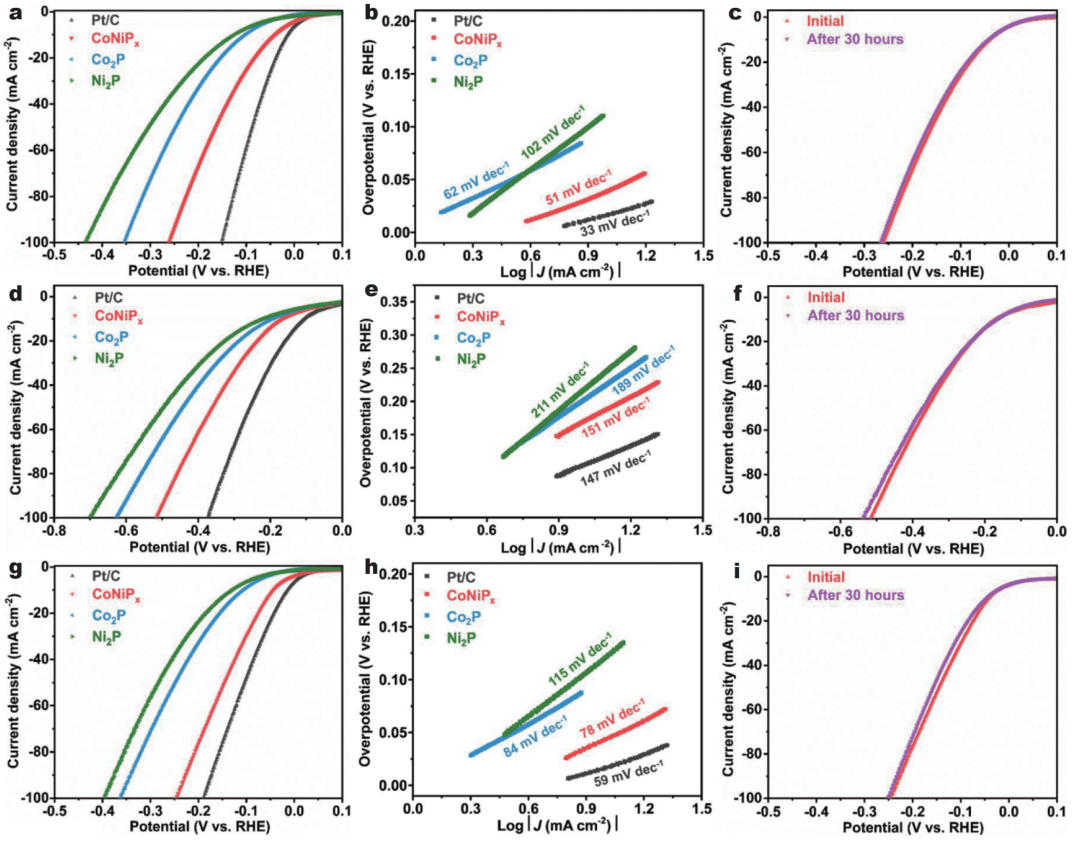

Figure 3 Linear sweep polarization curves obtained in (a) 0.5 mol L^{-1} H_2SO_4, (d) 1.0 mol L^{-1} PBS, and (g) 1.0 mol L^{-1} KOH. (b, e, h) The corresponding Tafel slopes of the HER polarization curves. (c, f, i) The comparison of HER polarization curves before and after 30 h measurements at −10 mA cm^{-2}.

(102 mV dec^{-1}). The significantly enhanced HER performance of the $CoNiP_x$ hollow nanocages may be attributed to the hollow structure and the synergistic effect of the Co and Ni inside. The overpotential and Tafel slope of the $CoNiP_x$ hollow nanocages obtained in 0.5 mol L^{-1} H_2SO_4 were compared with the recently reported non-noble metal electrocatalysts in Table S1, and they are comparable or superior to these electocatalysts. To further investigate the influence of electrochemically active surface area (ECSA) on the HER performance, the electrochemical double layer capacitance (C_{dl}) of the catalyst was estimated by conducting cyclic voltammetry (CV) measurements with different scan rates in non-Faradaic interval. As exhibited in Fig. S10, the C_{dl} of $CoNiP_x$ is 31.5 mF cm^{-2}, which is larger than those of Co_2P (24.4 mF cm^{-2}) and Ni_2P (21.7 mF cm^{-2}), indicating more exposed reaction active sites of the $CoNiP_x$ hollow nanocages for HER. The HER specific activities of $CoNiP_x$, Co_2P and Ni_2P were normalized by ECSA and compared in Fig. S11. The distance between the LSV curves are smaller than those in Fig. 3a, indicating a decreased activity gap between the catalysts. This result further proves that the ECSA plays an important role in the HER activity, but not the only dominant factor. The specific activity of the $CoNiP_x$ hollow nanocages is still better than those of Co_2P and Ni_2P, which reveals an intrinsic activity of the $CoNiP_x$. To further gain insight into the catalytic kinetics and interfacial properties of the electrocatalysts for HER, EIS measurements were conducted in 0.5 mol L^{-1} H_2SO_4 with an overpotential of 200 mV. As exhibited in Fig. S12, the $CoNiP_x$ exhibits the smallest diameter of the Nyquist plot semicircles, indicating the best electrical conductivity, fastest charge transfer and most favorable reaction kinetics. These results further demonstrate the hollow nanostructures can significantly decrease the ion transport resistance and ion diffusion length. The durability is a crucial factor for the electrocatalyst, and the stability of $CoNiP_x$ for HER in 0.5 mol L^{-1} H_2SO_4 was performed through the chronopotentiometry (CA) technique to maintain a current

density of −10 mA cm^{-2}. After 30 h measurement, a slight decrease can be observed in Fig. 3c and Fig. S13a, suggesting a long-term catalytic durability of $CoNiP_x$ for HER in 0.5 mol L^{-1} H_2SO_4.

The electrocatalytic HER performance of the $CoNiP_x$ towards HER in 1.0 mol L^{-1} PBS was also tested and the LSV curve is compared with the commercial 20% Pt/C, Co_2P and Ni_2P in Fig. 3d. The overpotential of these electrocatalysts at −10 mA cm^{-2} are 105, 166, 196 and 217 mV, respectively. Except the commercial 20% Pt/C, the $CoNiP_x$ shows the smallest overpotential value, revealing a better HER activity of $CoNiP_x$ than Co_2P and Ni_2P in neutral media. In addition, the Tafel slop of $CoNiP_x$ (Fig. 3e) is 151 mV dec^{-1}, which is very close to the commercial Pt/C (147 mV dec^{-1}) and much smaller than those of Co_2P (189 mV dec^{-1}) and Ni_2P (211 mV dec^{-1}), suggesting a more favorable HER kinetics of $CoNiP_x$. After 30 h running at −10 mA cm^{-2} in 1.0 mol L^{-1} PBS, the overpotential value of $CoNiP_x$ in Fig. S13b almost keeps the same with the initial value, and the HER LSV curve exhibits a tiny shift towards negative direction, indicating an excellent stability of $CoNiP_x$ for HER in neutral electrolyte. Compared with the reported noble-metal-free electrocatalysts in neutral media shown in Table S2, the catalytic activity of $CoNiP_x$ surpasses most of the reported materials. Similarly, the LSV curves of $CoNiP_x$, Co_2P, Ni_2P and the commercial 20% Pt/C obtained in 1.0 mol L^{-1} KOH with 10 mV s^{-1} scan rate were compared in Fig. 3g, in which $CoNiP_x$ reveals a overpotential of 52 mV, and it is much lower than those of Co_2P (108 mV) and Ni_2P (129 mV), exhibiting a higher HER activity of $CoNiP_x$. In Fig. 3h, the Tafel slop of $CoNiP_x$ is 78 mV dec^{-1}, which is larger than 59 mV dec^{-1} of the commercial 20% Pt/C and smaller than 84 mV dec^{-1} of Co_2P and 115 mV dec^{-1} of Ni_2P, further proving the better catalytic activity and reaction kinetics of $CoNiP_x$ in alkaline electrolyte. The durability test at −10 mA cm^{-2} shown in Fig. S13c indicates a good stability of $CoNiP_x$, the almost coincide LSV curves in Fig. 3i further demonstrates the strong durability of $CoNiP_x$ in alkaline media. The overpotential and Tafel slope of $CoNiP_x$ were compared with the similar electrocatalysts in Table S3, and smaller than most of the contrast materials. In conclusion, owing to the unique hollow structure and the synergistic effect between cobalt and nickel phosphides, the prepared $CoNiP_x$ hollow nanocages exhibit an outstanding HER activity in all-pH electrolyte.

The OER catalytic activity of $CoNiP_x$ was investigated in 1.0 mol L^{-1} KOH, and the linear sweep polarization curve was compared with the Co_2P, Ni_2P and the commercial IrO_2 in Fig. 4a. As shown in Fig. 4a, the obvious oxidation peaks at around 1.35 V can be observed in the LSV curves of $CoNiP_x$, Co_2P and Ni_2P, which are ascribed to the redox reactions of Co^{2+}/Co^{3+} and Ni^{2+}/Ni^{3+} in these catalysts [47,48]. To avoid the effects of these oxidation peaks, the current density of 50 mA cm^{-2} was selected and used as the evolution criterion. The η of $CoNiP_x$ at 50 mA cm^{-2} is 320 mV, which is close to 310 mV of the commercial IrO_2 and much smaller than 390 mV of Co_2P and 393 mV of Ni_2P, suggesting an excellent OER catalytic activity of $CoNiP_x$. As shown in Fig. 4b, the Tafel slops of $CoNiP_x$, Co_2P and Ni_2P are 140, 197 and 142 mV dec^{-1}, respectively, and the smallest Tafel slop of $CoNiP_x$ indicates a more favorable OER kinetics. Moreover, the overpotential and Tafel slop of $CoNiP_x$ are comparable or superior to most of the similar reported electrocatalysts (Table S4). EIS in Fig. 4c displays a lower transfer resistance of $CoNiP_x$ (10 Ω) than those of Co_2P (13.7 Ω) and Ni_2P (16Ω), which reveals a faster charge transfer and more favorable OER kinetics of $CoNiP_x$. To investigate the stability of $CoNiP_x$ for OER in 1.0 mol L^{-1} KOH, long-term measurement was performed (Fig. 4d). After 30 h, the current density of $CoNiP_x$ almost keeps the same, and the LSV curve is nearly coincident with the original one (Fig. 4d), indicating an outstanding stability for OER.

According to the excellent electrocatalytic activities of $CoNiP_x$ for both HER and OER, the overall water-splitting with $CoNiP_x$ as bifunctional electrocatalyst in both anode and cathode was conducted in 1.0 mol L^{-1} KOH. As exhibited in Fig. 4e, at a current density of 20 mA cm^{-2}, the cell voltage is as low as 1.61 V, which is a little larger than that of the commercial IrO_2(+)//Pt/C(−) (1.56 V), and comparable or superior to most recently reported bifunctional electrocatalysts (Table S5). During the water electrolysis, plenty of H_2 and O_2 bubbles can be obviously observed on the surfaces of the cathode and anode, respectively (Fig. 4f). Moreover, the long-term durability measurement was performed at 10 mA cm^{-2}, and the cell voltage can keep constant after 12 h (Fig. 4f). The HAADF-STEM image and the corresponding EDS elemental mapping images of the $CoNiP_x$ hollow nanocages after long-term durability measurement are shown in Fig. S14, in which the homogeneously distributed Co, Ni and P can be observed in the whole structure, further indicating a good stability of the $CoNiP_x$ hollow nanocages. The superior bifunctional electrocatalytic performance of the $CoNiP_x$ hollow nanocages is mainly ascribed to their structural characteristics. The numerous curved nanosheets on the surface significantly increase the

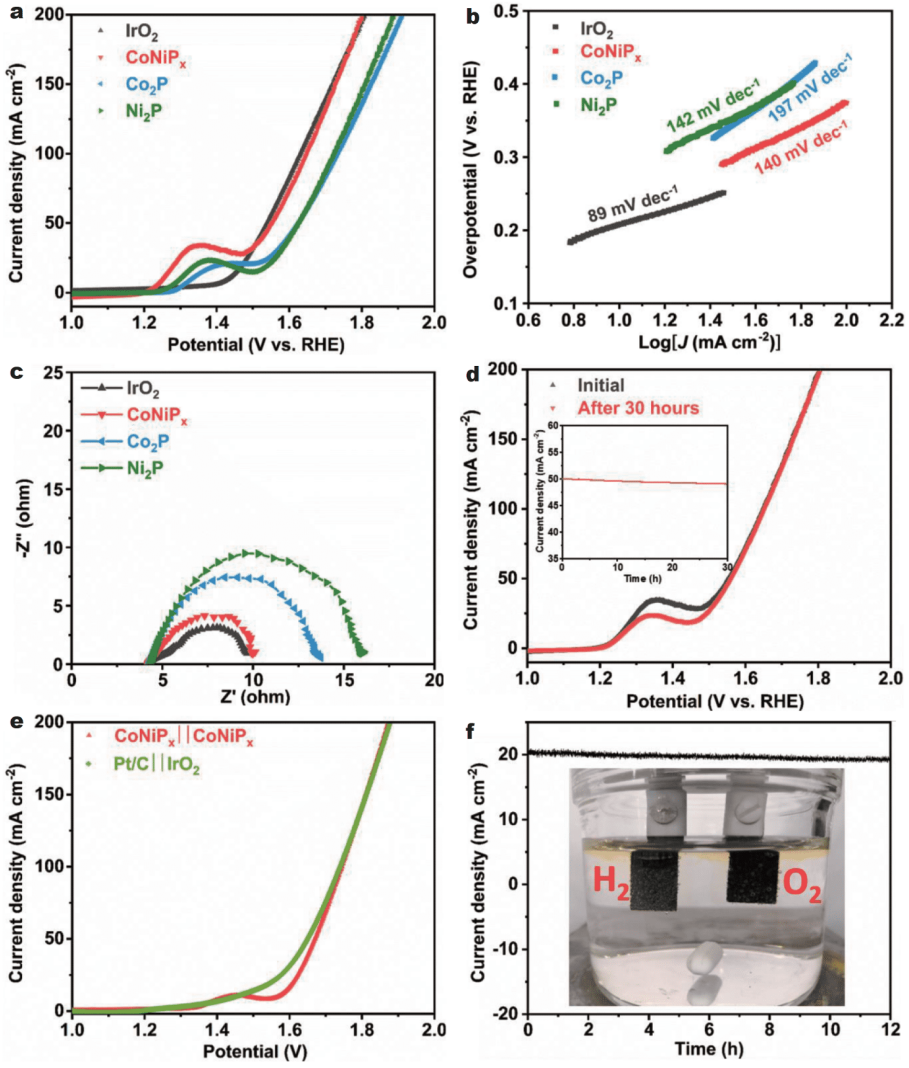

Figure 4 (a) OER linear sweep polarization curves obtained in 1.0 mol L^{-1} KOH with a scan rate of 10 mV s^{-1}. (b) The corresponding Tafel slopes of OER polarization curves. (c) EIS Nyquist plots of IrO_2, $CoNiP_x$, Co_2P and Ni_2P in 1.0 mol L^{-1} KOH from 100 kHz to 0.01 Hz. (d) The comparison of OER polarization curves before and after 30 h measurements at −50 mA cm^{-2}. Inset: the durability measurement of OER in 1.0 mol L^{-1} KOH. (e) LSV curves of a two-electrode alkaline electrolyzer for water electrolysis at a sweep rate of 5 mV s^{-1} in 1.0 mol L^{-1} KOH. (f) Long-term stability test conducted at a constant voltage of 1.61 V (the inset is the optical photograph showing the generation of H_2 and O_2 bubbles on the electrodes).

number of active sites to catalyze the HER and OER, and the hollow structure can accelerate the mass transfer and decrease the ion diffusion length. In addition, the synergistic effects between cobalt phosphide and nickel phosphide would facilitate the electron transfer during the HER and OER.

CONCLUSIONS

In summary, the hollow structured $CoNiP_x$ nanocages have been successfully synthesized *via* a self-templated strategy followed by an *in-situ* phosphorization. Benefiting from the unique hollow structure and bimetallic synergistic effects, the as-synthesized $CoNiP_x$ hollow nanocages exhibit an excellent electrocatalytic activity towards HER in all-pH electrolyte and a remarkable OER electrochemical performance in 1.0 mol L^{-1} KOH. Additionally, high stabilities for both HER and OER are also proved by the long-term durability measurements. Moreover, as the bifunctional electrocatalyst in both anode and cathode for overall water-splitting, the cell can achieve a current density of 10 mA cm^{-2} with a low voltage, and also a superior stability. This work can enrich

the bifunctional electrocatalysts for overall water-splitting, and provide a reference for further design and synthesis of bifunctional electrocatalysts for HER and OER.

Received 7 July 2020; accepted 30 July 2020; published online 30 September 2020

1 Cano ZP, Banham D, Ye S, *et al.* Batteries and fuel cells for emerging electric vehicle markets. Nat Energy, 2018, 3: 279–289
2 Zhang H, Nai J, Yu L, *et al.* Metal-organic-framework-based materials as platforms for renewable energy and environmental applications. Joule, 2017, 1: 77–107
3 Lu S, Zhuang Z. Electrocatalysts for hydrogen oxidation and evolution reactions. Sci China Mater, 2016, 59: 217–238
4 Turner JA. Sustainable hydrogen production. Science, 2004, 305: 972–974
5 Stern LA, Feng L, Song F, *et al.* Ni_2P as a Janus catalyst for water splitting: the oxygen evolution activity of Ni_2P nanoparticles. Energy Environ Sci, 2015, 8: 2347–2351
6 Li FL, Shao Q, Huang X, *et al.* Nanoscale trimetallic metal-organic frameworks enable efficient oxygen evolution electrocatalysis. Angew Chem Int Ed, 2018, 57: 1888–1892
7 Pan Y, Zhang C, Lin Y, *et al.* Electrocatalyst engineering and structure-activity relationship in hydrogen evolution reaction: From nanostructures to single atoms. Sci China Mater, 2020, 63: 921–948
8 Chen D, Pu Z, Lu R, *et al.* Ultralow Ru loading transition metal phosphides as high-efficient bifunctional electrocatalyst for a solar-to-hydrogen generation system. Adv Energy Mater, 2020, 10: 2000814
9 Huang Y, Gong Q, Song X, *et al.* Mo_2C nanoparticles dispersed on hierarchical carbon microflowers for efficient electrocatalytic hydrogen evolution. ACS Nano, 2016, 10: 11337–11343
10 Luo Z, Tan C, Lai Z, *et al.* A simple electrochemical method for conversion of Pt wires to Pt concave icosahedra and nanocubes on carbon paper for electrocatalytic hydrogen evolution. Sci China Mater, 2019, 62: 115–121
11 Chen Y, Li Z, Zhu Y, *et al.* Atomic Fe dispersed on N-doped carbon hollow nanospheres for high-efficiency electrocatalytic oxygen reduction. Adv Mater, 2019, 31: 1806312
12 Zhou G, Li M, Li Y, *et al.* Regulating the electronic structure of CoP nanosheets by O incorporation for high-efficiency electrochemical overall water splitting. Adv Funct Mater, 2019, 30: 1905252
13 Jiao Y, Zheng Y, Jaroniec M, *et al.* Design of electrocatalysts for oxygen- and hydrogen-involving energy conversion reactions. Chem Soc Rev, 2015, 44: 2060–2086
14 Zhu L, Lin H, Li Y, *et al.* A rhodium/silicon co-electrocatalyst design concept to surpass platinum hydrogen evolution activity at high overpotentials. Nat Commun, 2016, 7: 12272
15 Suen NT, Hung SF, Quan Q, *et al.* Electrocatalysis for the oxygen evolution reaction: recent development and future perspectives. Chem Soc Rev, 2017, 46: 337–365
16 Fang Z, Peng L, Lv H, *et al.* Metallic transition metal selenide holey nanosheets for efficient oxygen evolution electrocatalysis. ACS Nano, 2017, 11: 9550–9557
17 Hou Y, Lohe MR, Zhang J, *et al.* Vertically oriented cobalt selenide/NiFe layered-double-hydroxide nanosheets supported on exfoliated graphene foil: an efficient 3D electrode for overall water splitting. Energy Environ Sci, 2016, 9: 478–483
18 Chia X, Pumera M. Characteristics and performance of two-dimensional materials for electrocatalysis. Nat Catal, 2018, 1: 909–921
19 Xiao Y, Tian C, Tian M, *et al.* Cobalt-vanadium bimetal-based nanoplates for efficient overall water splitting. Sci China Mater, 2016, 61: 80–90
20 Yuan S, Pu Z, Zhou H, *et al.* A universal synthesis strategy for single atom dispersed cobalt/metal clusters heterostructure boosting hydrogen evolution catalysis at all pH values. Nano Energy, 2019, 59: 472–480
21 Li Y, Zhang H, Jiang M, *et al.* Ternary NiCoP nanosheet arrays: An excellent bifunctional catalyst for alkaline overall water splitting. Nano Res, 2016, 9: 2251–2259
22 He P, Yu XY, Lou XWD. Carbon-incorporated nickel-cobalt mixed metal phosphide nanoboxes with enhanced electrocatalytic activity for oxygen evolution. Angew Chem Int Ed, 2017, 56: 3897–3900
23 Gao WK, Yang M, Chi JQ, *et al.* *In situ* construction of surface defects of carbon-doped ternary cobalt-nickel-iron phosphide nanocubes for efficient overall water splitting. Sci China Mater, 2019, 62: 1285–1296
24 Huang Y, Li M, Yang W, *et al.* 3D ordered mesoporous cobalt ferrite phosphides for overall water splitting. Sci China Mater, 2020, 63: 240–248
25 Wang DY, Gong M, Chou HL, *et al.* Highly active and stable hybrid catalyst of cobalt-doped FeS_2 nanosheets–carbon nanotubes for hydrogen evolution reaction. J Am Chem Soc, 2015, 137: 1587–1592
26 Yi JD, Liu TT, Huang YB, *et al.* Solid-state synthesis of MoS_2 nanorod from molybdenum-organic framework for efficient hydrogen evolution reaction. Sci China Mater, 2019, 62: 965–972
27 Jia X, Zhao Y, Chen G, *et al.* Ni_3FeN nanoparticles derived from ultrathin NiFe-layered double hydroxide nanosheets: an efficient overall water splitting electrocatalyst. Adv Energy Mater, 2016, 6: 1502585
28 Yan M, Mao K, Cui P, *et al.* *In situ* construction of porous hierarchical $(Ni_{3-x}Fe_x)FeN$/Ni heterojunctions toward efficient electrocatalytic oxygen evolution. Nano Res, 2020, 13: 328–334
29 Gao MR, Liang JX, Zheng YR, *et al.* An efficient molybdenum disulfide/cobalt diselenide hybrid catalyst for electrochemical hydrogen generation. Nat Commun, 2015, 6: 5982
30 Hussain N, Wu F, Xu L, *et al.* $Co_{0.85}Se$ hollow spheres constructed of ultrathin 2D mesoporous nanosheets as a novel bifunctional-electrode for supercapacitor and water splitting. Nano Res, 2019, 12: 2941–2946
31 Wang P, Pu Z, Li W, *et al.* Coupling $NiSe_2$-Ni_2P heterostructure nanowrinkles for highly efficient overall water splitting. J Catal, 2019, 377: 600–608
32 Zhang Y, Li N, Zhang Z, *et al.* Programmable synthesis of multimetallic phosphide nanorods mediated by core/shell structure formation and conversion. J Am Chem Soc, 2020, 142: 8490–8497
33 Li J, Xia Z, Zhou X, *et al.* Quaternary pyrite-structured nickel/cobalt phosphosulfide nanowires on carbon cloth as efficient and robust electrodes for water electrolysis. Nano Res, 2017, 10: 814–825
34 Ji L, Wang J, Teng X, *et al.* CoP nanoframes as bifunctional electrocatalysts for efficient overall water splitting. ACS Catal, 2020, 10: 412–419
35 Zhang J, Yu L, Chen Y, *et al.* Designed formation of double-shelled

Ni-Fe layered-double-hydroxide nanocages for efficient oxygen evolution reaction. Adv Mater, 2020, 32: 1906432
36 Huang K, Sun Y, Zhang Y, *et al.* Hollow-structured metal oxides as oxygen-related catalysts. Adv Mater, 2019, 31: 1801430
37 Prieto G, Tüysüz H, Duyckaerts N, *et al.* Hollow nano- and microstructures as catalysts. Chem Rev, 2016, 116: 14056–14119
38 Yu L, Yang JF, Guan BY, *et al.* Hierarchical hollow nanoprisms based on ultrathin Ni-Fe layered double hydroxide nanosheets with enhanced electrocatalytic activity towards oxygen evolution. Angew Chem Int Ed, 2018, 57: 172–176
39 Wang H, Zhang X, Wang J, *et al.* Puffing quaternary $Fe_xCo_yNi_{1-x-y}P$ nanoarray via kinetically controlled alkaline etching for robust overall water splitting. Sci China Mater, 2020, 63: 1054–1064
40 Shi H, Liang H, Ming F, *et al.* Efficient overall water-splitting electrocatalysis using lepidocrocite VOOH hollow nanospheres. Angew Chem Int Ed, 2017, 56: 573–577
41 Li Z, Han F, Li C, *et al.* Multi-anion intercalated layered double hydroxide nanosheet-assembled hollow nanoprisms with improved pseudocapacitive and electrocatalytic properties. Chem Asian J, 2018, 13: 1129–1137
42 Lv JJ, Wu S, Qiao M, *et al.* Mesoporous $NiCoP_x$ nanoplates as highly efficient electrocatalysts for overall water splitting. J Power Sources, 2018, 400: 434–440
43 Zhang R, Wang X, Yu S, *et al.* Ternary $NiCo_2P_x$ nanowires as pH-universal electrocatalysts for highly efficient hydrogen evolution reaction. Adv Mater, 2017, 29: 1605502
44 Liu C, Zhang G, Yu L, *et al.* Oxygen doping to optimize atomic hydrogen binding energy on NiCoP for highly efficient hydrogen evolution. Small, 2018, 14: 1800421
45 Yan L, Zhang B, Zhu J, *et al.* Electronic modulation of cobalt phosphide nanosheet arrays *via* copper doping for highly efficient neutral-pH overall water splitting. Appl Catal B-Environ, 2020, 265: 118555
46 Fan H, Liu H, Hu X, *et al.* Fe_2P@mesoporous carbon nanosheets synthesized *via* an organic template method as a cathode electrocatalyst for Zn-air batteries. J Mater Chem A, 2019, 7: 11321–11330
47 Jin Y, Huang S, Yue X, *et al.* Mo- and Fe-Modified $Ni(OH)_2$/NiOOH nanosheets as highly active and stable electrocatalysts for oxygen evolution reaction. ACS Catal, 2018, 8: 2359–2363
48 Chen S, Kang Z, Hu X, *et al.* Delocalized spin states in 2D atomic layers realizing enhanced electrocatalytic oxygen evolution. Adv Mater, 2017, 29: 1701687

Acknowledgements This work was supported by the National Key R&D Program of China (2017YFA 0208300 and 0700104), the National Natural Science Foundation of China (21671180) and the State Key Laboratory of Organic Inorganic Composites (oic-201801007).

Author contributions Yu ZQ and Wu Y designed the materials; Wang Z and Yang J performed the experiments; Wang W and Zhou F helped to analyze the data; Zhou H, Xue Z and Xiong C modified the manuscript; All authors contributed to the general discussion.

Conflict of interest The authors declare no conflict of interest.

Supplementary information Experimental details and supporting data are available in the online version of the paper.

Zhiyuan Wang obtained his PhD in physical chemistry at RWTH Aachen University, Germany, in 2018. He then carried out postdoctoral research with Prof. Yuen Wu at iChEM (Collaborative Innovation Center of Chemistry for Energy Materials), University of Science and Technology of China. His research focuses on the synthesis of nanomaterials and their applications in photocatalysis and electrocatalysis.

Yuen Wu received his BSc and PhD degrees from the Department of Chemistry, Tsinghua University in 2009 and 2014, respectively. He is currently a professor in the Department of Chemistry, University of Science and Technology of China. His research interests are focused on the synthesis, assembly, characterization and application exploration of functional nanomaterials.

钴-镍双金属磷化物中空纳米笼用于高效电解水

王志远[1,2], 杨佳[2], 王文玉[2], 周方耀[2], 周煌[2], 薛正刚[2], 熊灿[2], 余振强[1*], 吴宇恩[2*]

摘要 制备一种低成本、高效、稳定耐用的双功能电催化剂对于电催化水分解至关重要. 本文采用自模板策略和原位磷化工艺相结合的方法构建了一种具有中空结构的钴镍双金属磷化物纳米笼($CoNiP_x$). 由于其独特的中空结构和钴镍双金属之间的协同效应, 合成的$CoNiP_x$中空纳米笼催化剂在全pH值范围的电解质中对析氢反应均表现出优异的电催化活性和稳定性, 并在1.0 mol L^{-1} 氢氧化钾(KOH)中对析氧反应也表现出很好的电化学性能. $CoNiP_x$中空纳米笼作为阳极和阴极的双功能催化剂也显示出了优异的全解水性能, 在20 mA cm^{-2}电流密度下, 电压值为1.61 V, 且稳定性良好.

